# Supporting Information

## A deep dive into mechanochemical organic reactions by accurate crystallographic analysis via TAAM refinement

Ana M. Constantin[a], Francesco Mele[a], Vinayak Botla[a], Nicola Della Ca'[a], Raimondo Maggi[a], Giovanni Maestri[a], Alessandro Cerveri[a], Remie M. Sundermann[a],Daniele Cauzzi[a], Francesco Pancrazzi*[a], Paolo P. Mazzeo*[a,b]

[a.] *Department of Chemistry, Life Sciences and Environmental Sustainability, Università di Parma, Parco Area delle Scienze 17/A, 43124 Parma, Italy. Email: paolopio.mazzeo@unipr.it; francesco.pancrazzi@unipr.it.*
[b.] *Biopharmanet-tec, Parco Area delle Scienze 95, 43124 Parma, Italy.*

# Optimization of reaction conditions

*General procedure for optimization reactions*

The optimization of the reaction conditions was carried out by studying the reaction of 8-aminoquinoline (**1**) and benzoyl peroxide to give N-(7-hydroxyquinolin-8-yl)benzamide (**3a**).

In a ball milling vessel (stainless steel, 15 mL), loaded with one grinding ball (stainless steel, diameter 15 mm) or two grinding balls (stainless steel, diameter 5 mm), was added sequentially 8-aminoquinoline (1 eq., 0.2 mmol, 28.8 mg) and benzoyl peroxide portion wise (see tables S1-S4). After all the reagents were added, the selected solvent was putted above. The vessel was closed in air and the jar was placed in the vibratory ball mill (Fritsch Pulverisette P23) at given milling frequency (see tables S1-S4) for the time specified. At the end of the reaction, the reaction mixture was recovered with EtOAc. The resulting reaction mixture was concentrated under reduced pressure and finally purified by flash column chromatography (eluent Hexane/EtOAc).

*Optimization of mechanochemical parameters*

**Table S1**. Optimization of the mechanochemical parameter

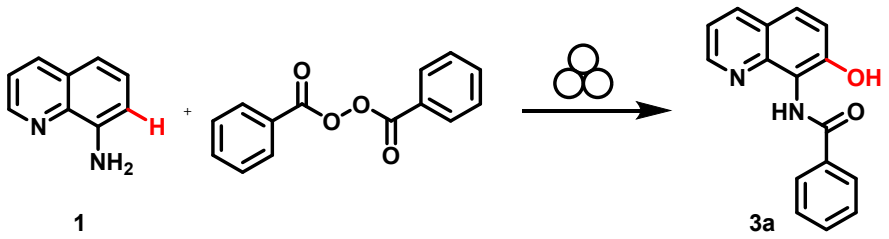


| *Entry* | *BPO (eq.)* | *Time* | *Frequency* | *Yield of 3a*[b] |
|---|---|---|---|---|
| 1 | 1.1 | 1h | 15 Hz | 10% |
| 2 | 1.1 | 2h | 15 Hz | 28% |
| 3 | 1.1 | 4h | 15 Hz | 10% |
| 4 | 1.5 | 2h | 15 Hz | 18% |
| 5 | 1.1 | 2h | 30 Hz | 21% |
| 6 | 1.1 (0.18x6) | 2h | 15 Hz | 30% |
| 7[a] | 1.1 (0.37x3) | 2h | 15 Hz | 35% |
| 8 | 1.5 (0.5x3) | 2h | 15 Hz | 50% |
| 9 | 1.1 (0.37x3) | 2h | 15 Hz | 55% |

[a]Two stainless steel balls of 5mm instead of one SS ball of 15mm. [b]Isolated yield

*Optimization of Liquid Assisted Grinding (LAG)*

**Table S2.** Optimization of LAG

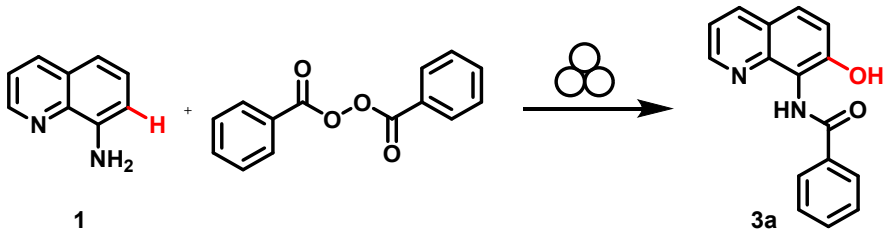


1 3a

| *Entry* | *BPO (eq.)* | *LAG (η)* | *Yield of 3a[a]* |
|---|---|---|---|
| 1 | 1.1 (0.37x3) | $H_2O$ (η=1) | 18% |
| 2 | 1.1 (0.37x3) | $H_2O$ (η=3) | 17% |
| 3 | 1.1 (0.37x3) | EtOAc (η=1) | 25% |
| 4 | 1.1 (0.37x3) | ACN (η=1) | 27% |

[a]Isolated yield

## Optimization of auxiliary additives

**Table S3.** Study of auxiliary additives

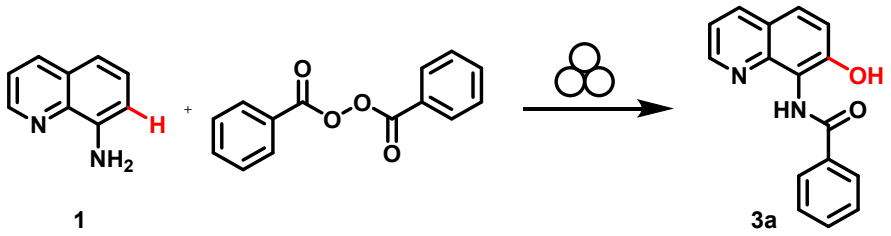


1 3a

| *Entry* | *BPO (eq.)* | *Additive* | *Yield of 3a[a]* |
|---|---|---|---|
| 1 | 1.1 (0.37x3) | $Na_2SO_4$ | 17% |
| 2 | 1.1 (0.37x3) | NaCl | 17% |
| 3 | 1.1 (0.37x3) | $SiO_2$ | 20% |

[a]Isolated yield

*Extension of the reaction conditions*

Following the general procedure, in a ball milling vessel (stainless steel, 15 mL) loaded with one grinding ball (stainless steel, diameter 15mm) was added sequentially 8-aminoquinoline (1 eq., 0.2 mmol, 28.8 mg) and di-(4-methylbenzoyl)peroxide portion wise (1.1 eq., 0.22 mmol in 3 times). After all the reagents were added the specified solvent was putted above. The vessel was closed in air and the jar was placed in the vibratory ball mill (Fritsch Pulverisette P23) at 15 Hz. At the end of the reaction, the reaction mixture was recovered with EtOAc. The resulting reaction mixture was concentrated under reduced pressure, and finally purified by flash column chromatography (eluent Hexane/EtOAc).

**Table S4.** Extension of the reaction conditions

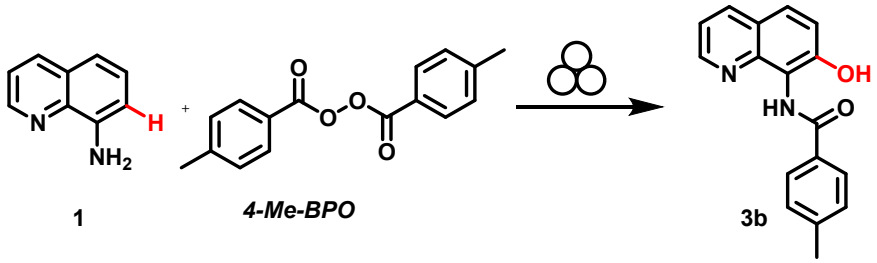


| *Entry* | *4-Me-BPO (eq.)* | *Time* | *Frequency* | *LAG* | *Yield of 3b*[a] |
|---|---|---|---|---|---|
| 1 | 1.5 | 2 h | 15 Hz | - | 10% |
| 2 | 1.5 | 2 h | 15 Hz | $H_2O$ (18 µL) | Traces |
| 3 | 1.5 | 2 h | 15 Hz | $H_2O$ (50 µL) | 23% |
| 4 | 1.5 | 2h | 15 Hz | EtOAc (300 µL) | 40% |

[a]Isolated yield

# Experimental procedures

### *General procedure for ball mill reaction*

In a ball milling vessel (stainless steel, 15 mL) loaded with one grinding ball (stainless steel, diameter 15mm, 13.5g) was added sequentially 8-aminoquinoline (1 eq., 0.2 mmol, 28.8 mg) and benzoyl peroxide portion wise (1.1 eq., 0.22 mmol in 3 times). After all the reagents were added the specified solvent was putted above. The vessel was closed in air and the jar was placed in the vibratory ball mill (Fritsch Pulverisette P23) at 15 Hz. At the end of the reaction, the reaction mixture was recovered with EtOAc or DCM. The resulting reaction mixture was concentrated under reduced pressure, and finally purified by flash column chromatography (eluent Hexane/EtOAc 15:1).

### *Control experiments: Reaction in zirconia jar*

To eliminate the possibility that metal leaching from the stainless-steel grinding jar could influence peroxide activation, control experiments were performed using a zirconia grinding jar as inert material.

Following the *general procedure* in a zirconia milling vessel ($ZrO_2$, 15 mL) loaded with one grinding ball (zirconia ball, diameter 15mm, 10 g) was added sequentially 8-aminoquinoline (1 eq., 0.2 mmol, 28.8 mg) and benzoyl peroxide portion wise (1.1 eq., 0.22 mmol in 3 times). The vessel was closed in air and the jar was placed in the vibratory ball mill (Fritsch Pulverisette P23) at 15 Hz. At the end of the reaction, the reaction mixture was recovered with EtOAc or DCM. The resulting reaction mixture was concentrated under reduced pressure and finally purified by flash column chromatography (eluent Hexane/EtOAc 15:1). Product **3a** was obtained in 32% yield.

This experiment demonstrated that the reaction proceeded similarly in both jar materials. Although the product yield was marginally lower when the reaction was conducted in a zirconia jar, this difference can likely be attributed to the differing hardness of the grinding media.

Collectively, these findings indicate that metal leaching from the stainless-steel jar had a negligible impact on the peroxide activation process.

### *Mechanistic considerations*

To exclude the possibility of an initial amide formation followed by oxidation of the quinoline ring by a peroxybenzoic acid intermediate, we conducted the following control experiments:

1) *Peroxyacid Oxidation*: N-(Quinolin-8-yl)benzamide (**4**) was treated with meta-chloroperoxybenzoic acid (mCPBA) under standard reaction conditions. No formation of N-(7-hydroxyquinolin-8-yl)benzamide (**3a**) was observed, and the starting material was recovered quantitatively.

2) *Benzoyl Peroxide Oxidation*: Compound **4** was directly treated with benzoyl peroxide (BPO) under the same reaction conditions. No formation of product **3a** was detected, indicating that BPO does not induce the desired oxidation on the pre-formed amide.

These control experiments collectively suggest that a stepwise mechanism involving initial amide formation and subsequent oxidation is unlikely. Instead, a concerted mechanism, where the oxidation at the C7 position occurs simultaneously with amide bond formation, is more plausible.

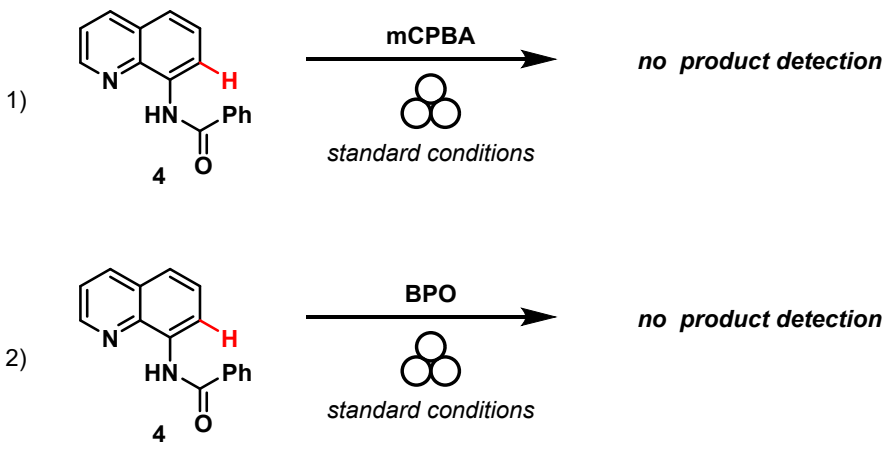


**Figure S1.** Control experiments.

# Characterization data

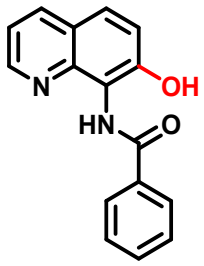


**N-(7-hydroxyquinolin-8-yl)benzamide** (**3a**). Prepared according to the *general procedure.* Pale yellow solid, (29.0 mg, yield 55%). mp: 98-99 °C.

**$^{1}$H NMR** (400 MHz, $CDCl_3$) δ 11.98 (s, 1H), 11.01 (s, 1H), 8.81 (dd, *J* = 4.4, 1.7 Hz, 1H), 8.14 (ddd, *J* = 8.3, 6.4, 1.5 Hz, 3H), 7.69 – 7.63 (m, 1H), 7.60 (dt, *J* = 8.8, 3.9 Hz, 3H), 7.39 – 7.31 (m, 2H).

**$^{13}$C NMR** (101 MHz, $CDCl_3$) δ 166.6, 148.8, 148.0, 141.2, 136.2, 133.2, 132.6, 129.0, 127.7, 125.2, 122.7, 122.6, 121.7, 119.2, 117.7.

*An HSQC spectrum was also taken to ascertain the coupling of the proton to the nitrogen atom. The spectra is displayed in the NMR spectra part.*

**[$^{1}$H,$^{15}$N] HSQC NMR** (600 MHz, 61 MHz, $CDCl_3$, 25°C): (δ 11.0, 117.9) ppm.

**HRMS (ESI)** m/z calculated for $C_{16}H_{12}N_2NaO_2^+$ $[M+Na]^+$: 287.0791, found: 287.0793.

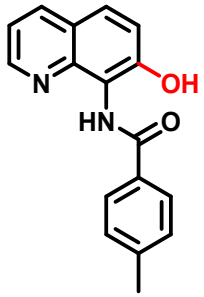


**N-(7-hydroxyquinolin-8-yl)-4-methylbenzamide** (**3b**). Prepared according to the *general procedure.* Pale yellow solid. (22.3 mg, yield 40%). mp: 147-149 °C.

**$^{1}$H NMR** (400 MHz, $CDCl_3$) δ 12.02 (s, 1H), 10.95 (s, 1H), 8.79 (dd, *J* = 4.3, 1.6 Hz, 1H), 8.11 (dd, *J* = 8.1, 1.6 Hz, 1H), 8.01 (dd, *J* = 8.6, 2.2 Hz, 2H), 7.57 (d, *J* = 8.9 Hz, 1H), 7.40 – 7.30 (m, 4H), 2.46 (d, *J* = 5.8 Hz, 3H).
**$^{13}$C NMR** (101 MHz, $CDCl_3$) δ 166.8, 148.9, 148.1, 143.4, 141.3, 136.3, 129.8, 127.8, 125.1, 122.9, 119.3, 117.9, 21.8.
**HRMS (ESI)** m/z calculated for $C_{17}H_{15}N_2NaO_2^+$ $[M+Na]^+$: 302.0791, found: 302.0794.

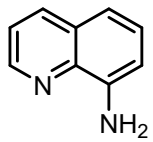


**[$^{1}$H,$^{15}$N] HSQC NMR of 8-aminoquinoline** (600 MHz, 61 MHz, $CDCl_3$, 25°C): (δ 5.0, 46.6) ppm.

# NMR spectra

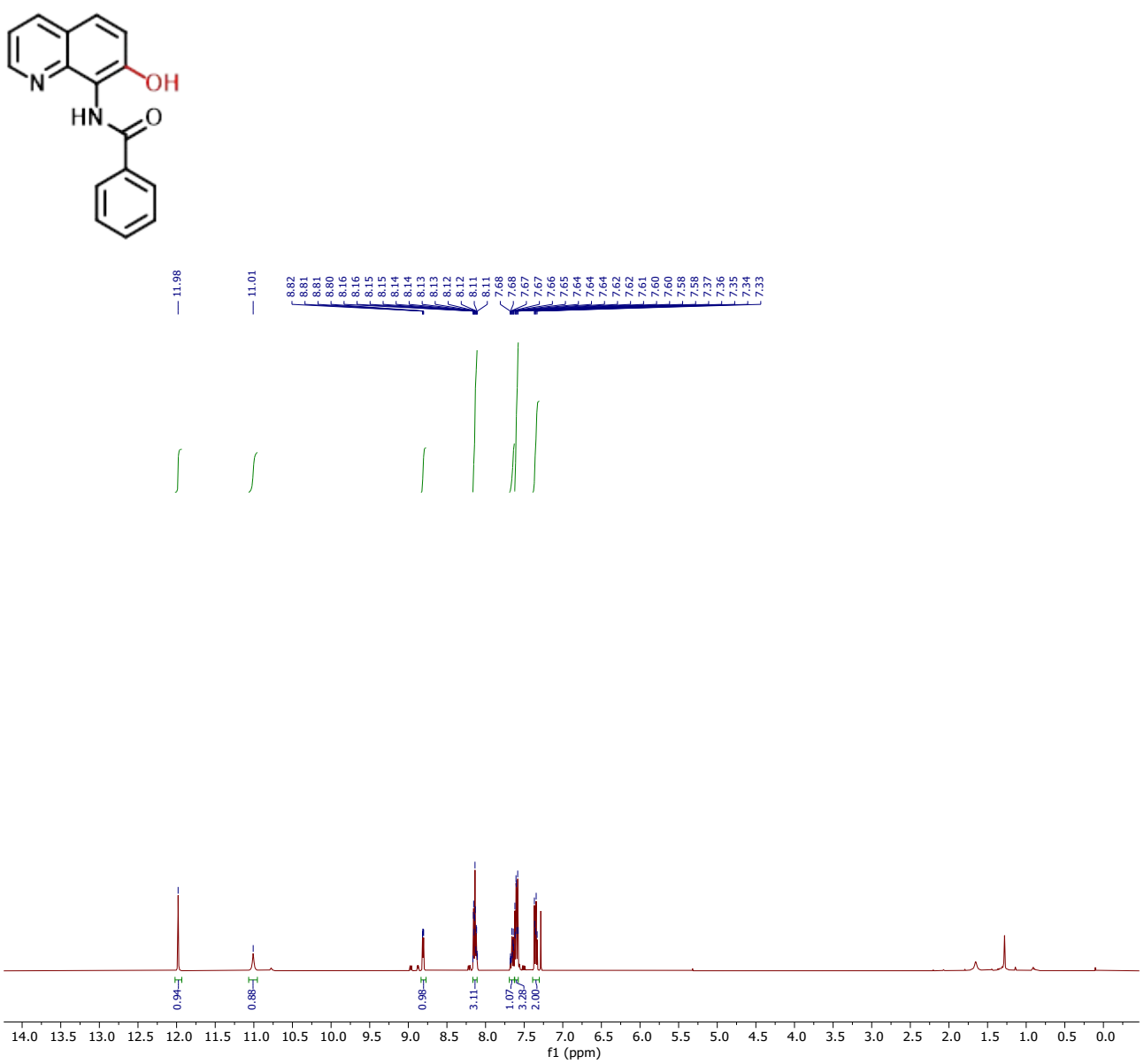


**Figure S2**· $^{1}$H NMR spectrum of compound **3a** (400 MHz, $CDCl_3$)

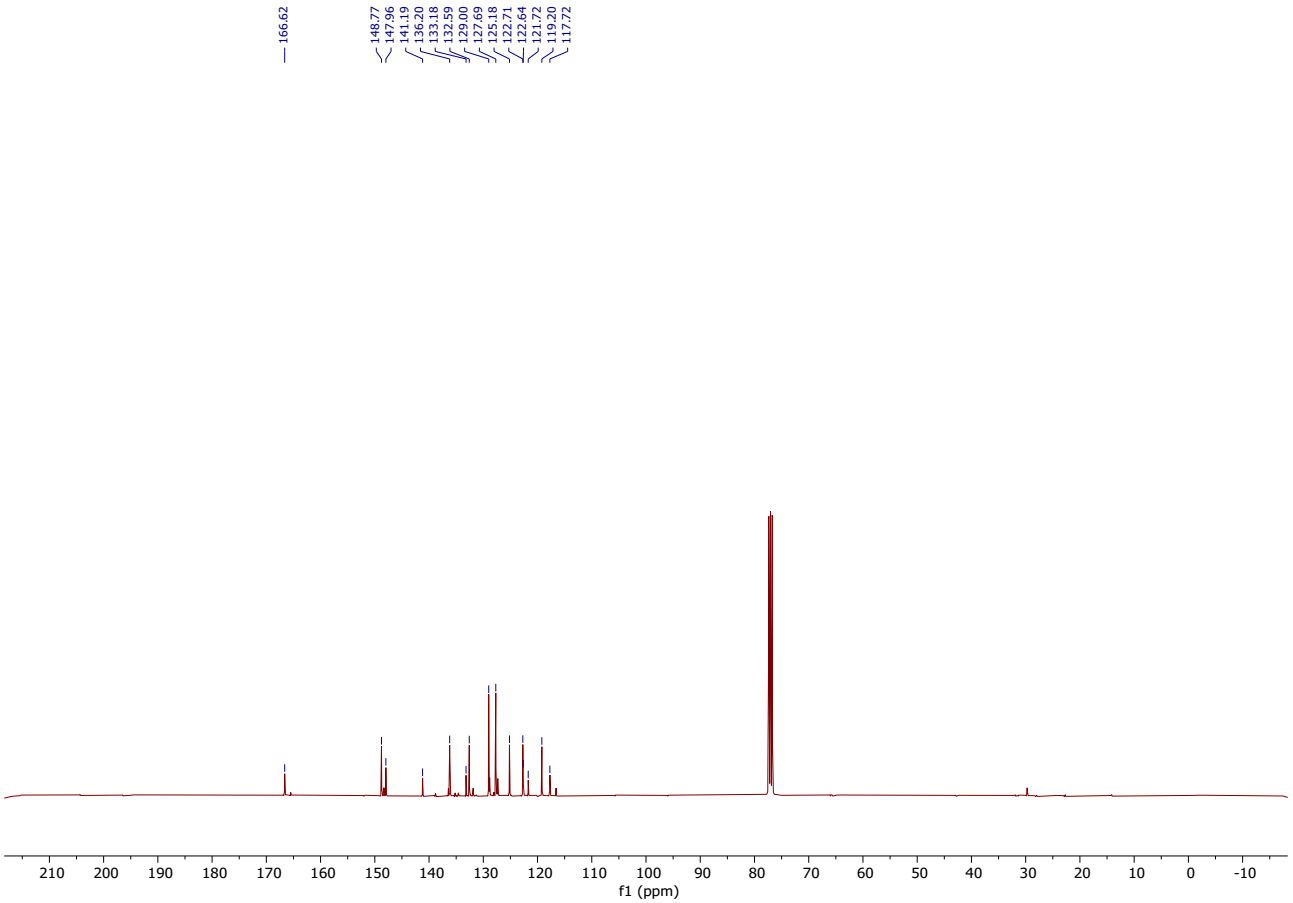


**Figure S3.** $^{13}C$ NMR spectrum of compound **3a** (101 MHz, $CDCl_3$)

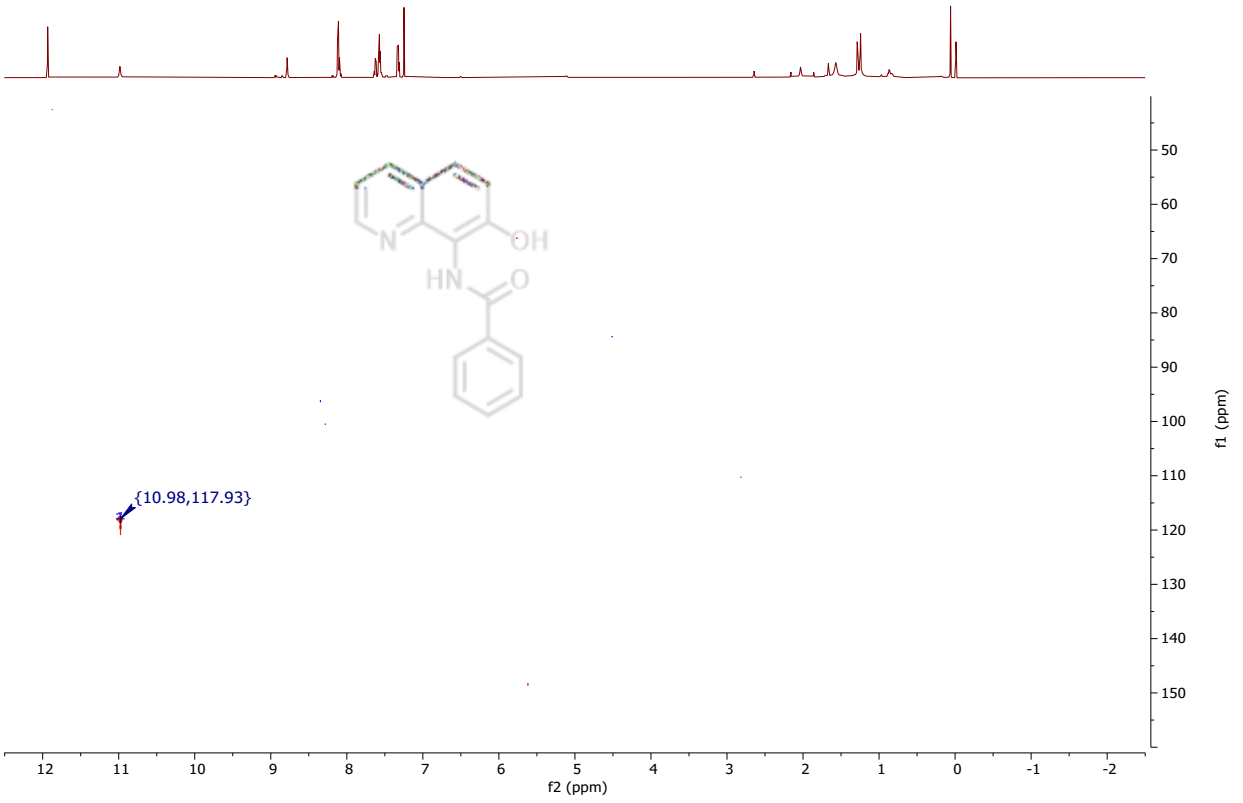


**Figure S4.** [$^{1}H$,$^{15}N$] HSQC NMR (600 MHz, 61 MHz, $CDCl_3$) of compound **3a**.

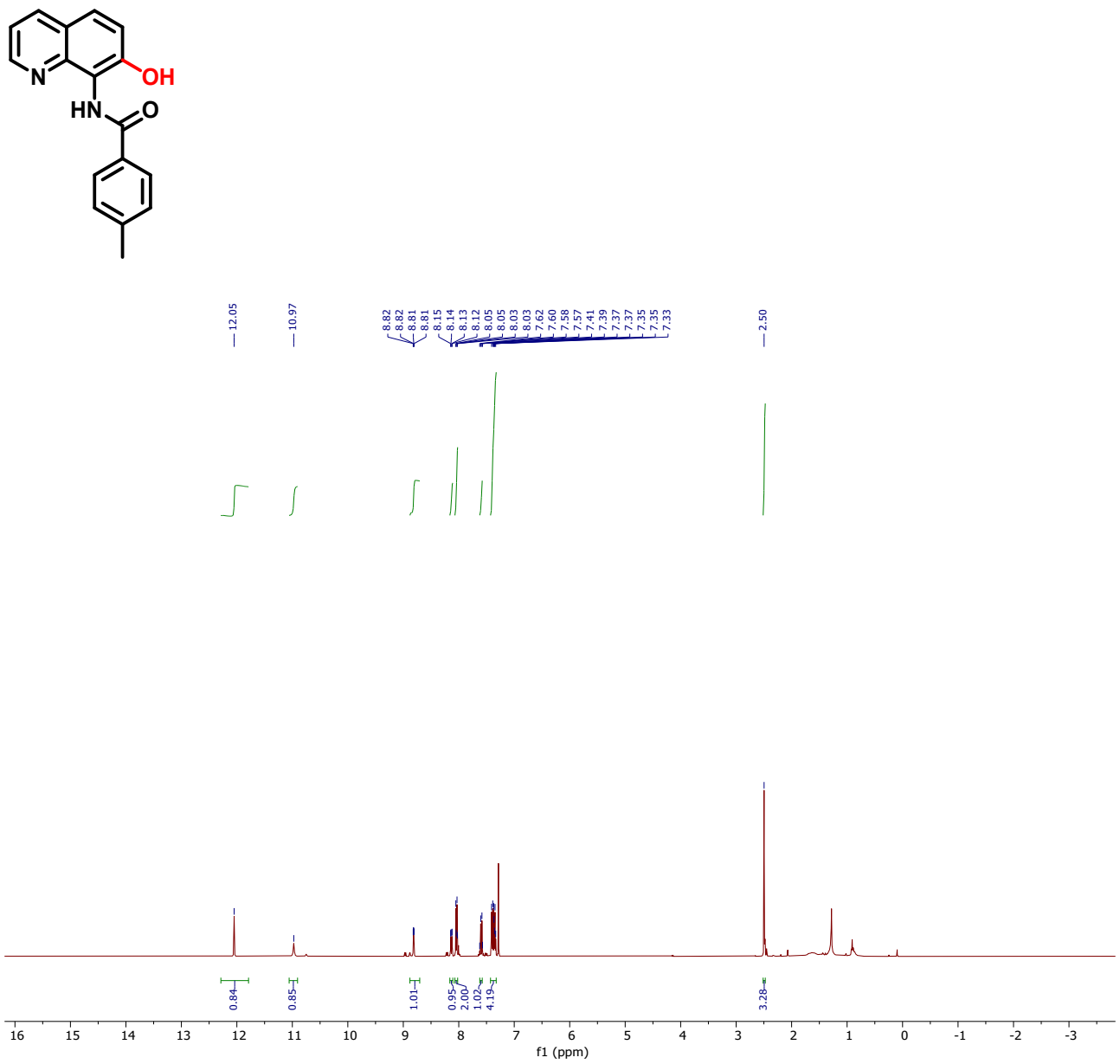


**Figure S5.**$^{1}$H NMR spectrum of compound **3b** (400 MHz, $CDCl_3$)

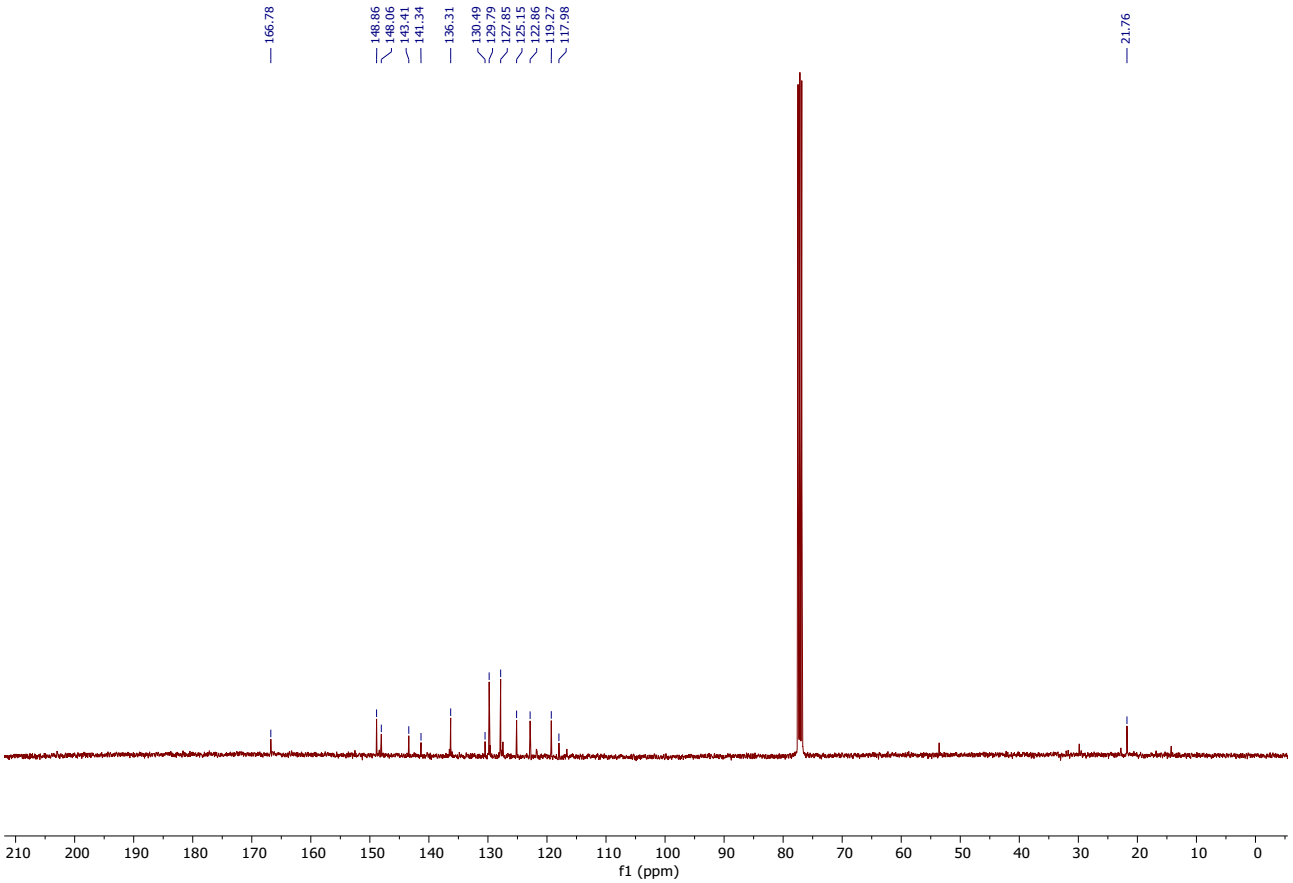


**Figure S6.** $^{13}$C NMR spectrum of compound **3b** (101 MHz, $CDCl_3$)

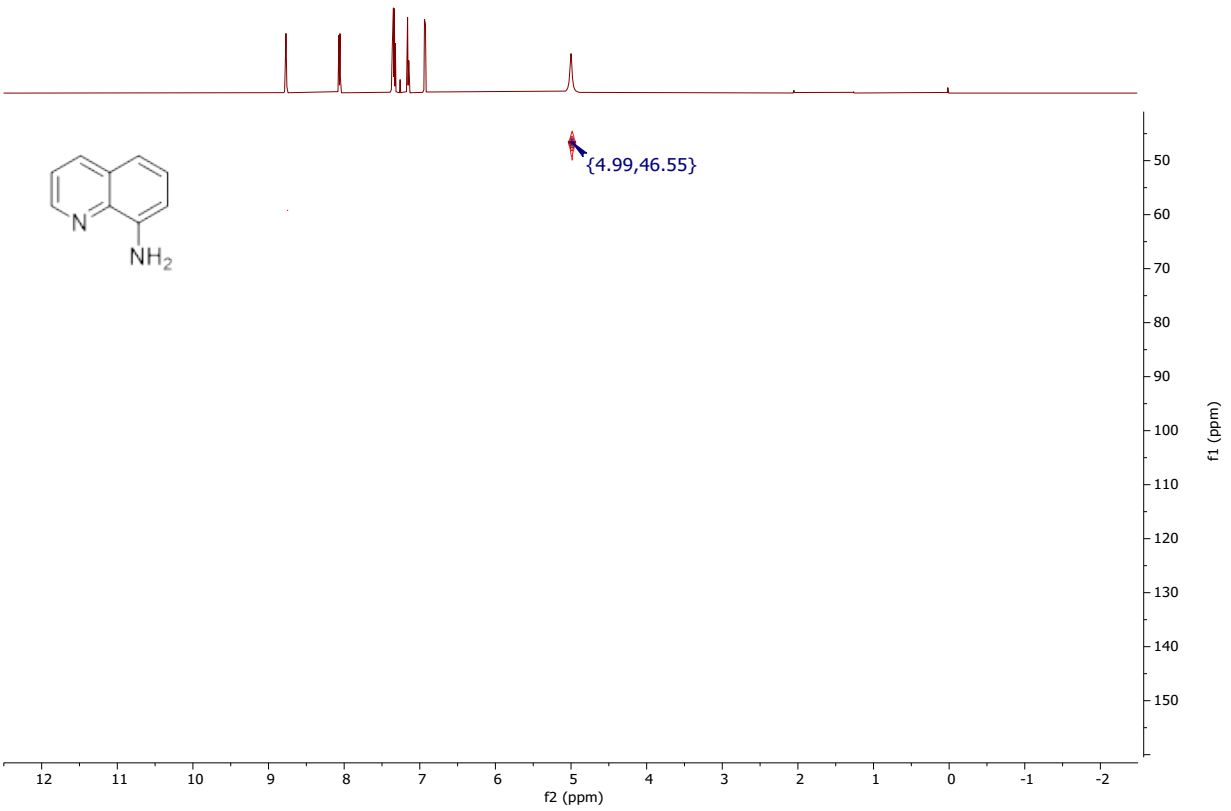


**Figure S7**. [$^{1}$H,$^{15}$N] HSQC NMR (600 MHz, 61 MHz, CDCl3) of 8-aminoquinoline.

# IR spectra

The HATR-FTIR analysis of the isolated compound (Figure **S8**) shows a single signal at 3281 $cm^{-1}$ attributable to the NH of an amide, while the signal for the OH could be attributed to the broad band centered at 2575 $cm^{-1}$, given the presence of a strong intramolecular hydrogen bond. There are no signals in the spectrum attributable to the presence of an aromatic $NH_2$, which generally presents two peaks of the same intensity in the spectral range above 3400 $cm^{-1}$. Observing the spectral range that characterizes carboxylic acid derivatives (Figure **S9**), there are two very intense bands at 1633 and 1528 $cm^{-1}$, which can reasonably be attributed to the amide I and amide II absorption bands, respectively[1]. The presence of an ester, on the other hand, is excluded by IR analysis, as diagnostic absorption bands in the ester region (in the range between 1800 and 1700 $cm^{-1}$)[2] are not present in the spectrum.

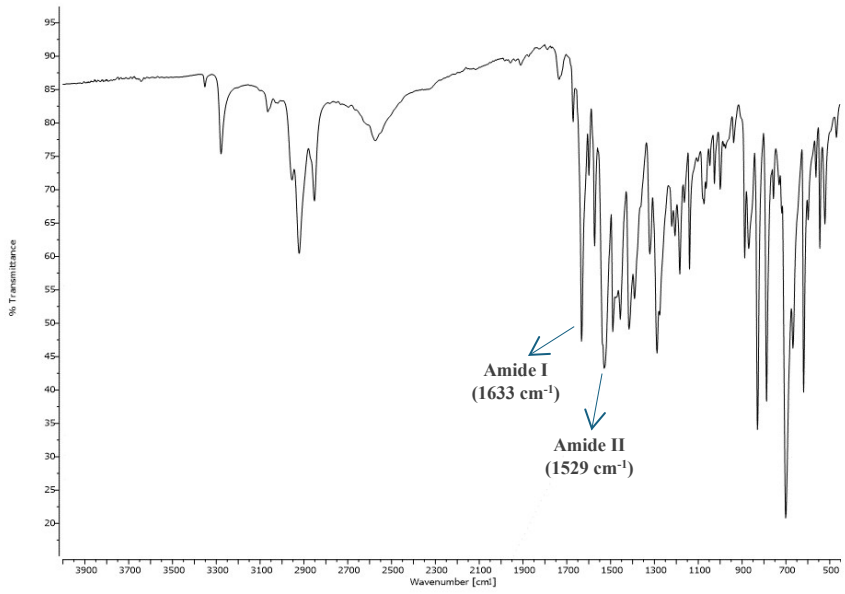


**Figure S8.** FTIR spectum of compound **3a**.

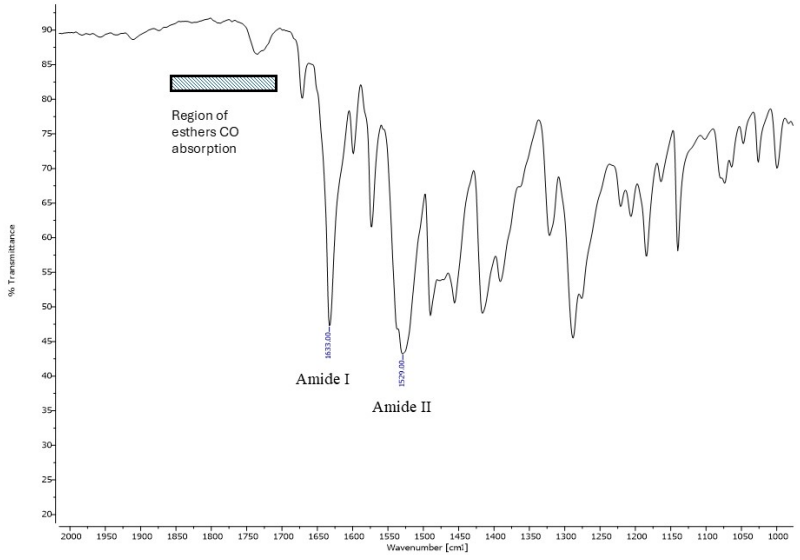


**Figure S9.** Enlarged view of the IR region corresponding to the characteristic amide functional group in Figure S8 of **3a** as reported int the main text Figure 3.

# Crystallography

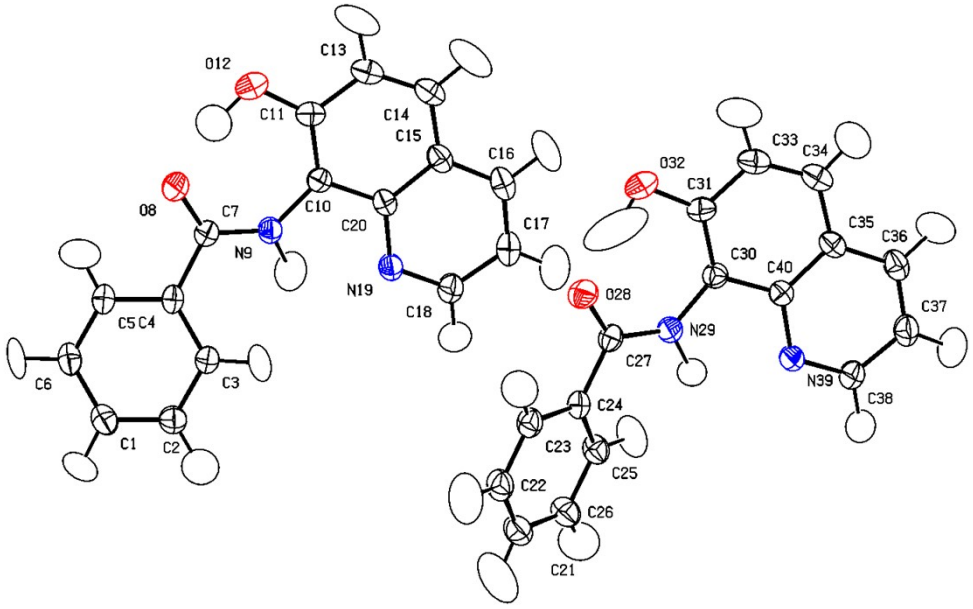


**Figure S10.** ORTEP drawing of the independent molecule of **3a** in the asymmetric unit. All atoms shown as ellipsoids as for a complete TAAM refinement, at the 50% probability level. Color code: grey=C, red=O, blue=N, white=H.

**Table S5.** Crystal data and structure refinement for **3a** and CCDC1559199 (original data vs. re-refined data)

| | | CCDC 1559199 | |
|---|---|---|---|
| **Identification code** | **3a** | **original** | **re-refined** |
| Empirical formula | $C_{16}H_{12}N_2O_2$ | $C_{17}H_{14}N_2O_2$ | $C_{17}H_{14}N_2O_2$ |
| Formula weight | 264.286 | 278.30 | 278.30 |
| Temperature/K | 200.00 | 294.15 | 294.15 |
| Crystal system | monoclinic | monoclinic | monoclinic |
| Space group | P21/c | $P2_1/c$ | $P2_1/c$ |
| a/Å | 14.5096(9) | 11.954(2) | 11.954(2) |
| b/Å | 17.8805(11) | 7.454(2) | 7.454(2) |
| c/Å | 10.3906(6) | 15.468(3) | 15.468(3) |
| α/° | 90 | 90 | 90 |
| β/° | 110.379(2) | 95.33(3) | 95.33(3) |
| γ/° | 90 | 90 | 90 |
| Volume/Å$^3$ | 2527.0(3) | 1372.4(5) | 1372.4(5) |
| Z | 8 | 4 | 4 |
| $\rho_{calc}$g/cm$^3$ | 1.389 | 1.347 | 1.347 |
| μ/mm$^{-1}$ | 0.094 | 0.090 | 0.090 |
| F(000) | 1104.7 | 584.0 | 584.0 |
| Crystal size/mm$^3$ | 0.8 × 0.1 × 0.08 | 0.42 × 0.38 × 0.24 | 0.42 × 0.38 × 0.24 |
| Radiation | Mo Kα (λ = 0.71073) | MoKα (λ = 0.71073) | MoKα (λ = 0.71073) |
| 2Θ range for data collection/° | 4.76 to 52.9 | 5.29 to 49.958 | 5.29 to 49.958 |
| Index ranges | -18 ≤ h ≤ 18,<br>-22 ≤ k ≤ 22,<br>-13 ≤ l ≤ 13 | -14 ≤ h ≤ 14,<br>-8 ≤ k ≤ 8,<br>-18 ≤ l ≤ 18 | -14 ≤ h ≤ 14,<br>-8 ≤ k ≤ 8,<br>-18 ≤ l ≤ 18 |
| Reflections collected | 50783 | 24733 | 24733 |
| Independent reflections | 4343<br>Rint = 0.0849<br>Rsigma = 0.0381 | 2413<br>$R_{int}$ = 0.0235<br>$R_{sigma}$ = 0.0143 | 2413<br>$R_{int}$ = 0.0235<br>$R_{sigma}$ = 0.0143 |
| Data/restraints/parameters | 4343/9/578 | 2413/0/192 | 2413/1/209 |
| Goodness-of-fit on F$^2$ | 1.151 | 1.060 | 1.055 |
| Final R indexes [I>=2σ (I)] | R1 = 0.0438<br>wR2 = 0.0861 | $R_1$ = 0.0696<br>$wR_2$ = 0.2049 | $R_1$ = 0.0390<br>$wR_2$ = 0.1119 |
| Final R indexes [all data] | R1 = 0.0560<br>wR2 = 0.0907 | $R_1$ = 0.0749<br>$wR_2$ = 0.2126 | $R_1$ = 0.0429<br>$wR_2$ = 0.1173 |
| Largest diff. peak/hole / e Å$^{-3}$ | 0.23/-0.21 | 0.50/-0.54 | 0.19/-0.12 |

*Crystallographic data refinement*

Crystallographic data deposited in the CCDC Crystal Structure database (CCDC 1559199 available free of charge from WebCSD website, https://www.ccdc.cam.ac.uk/structures) have been downloaded to directly compare our results with those discussed by Botla et al. in 2019. Data were solved with a $R_1$ = 6.96 with the largest difference peak of 0.50 eÅ$^{-3}$ and the largest difference hole of -0.54 eÅ$^{-3}$. The misinterpretation of the heteroatom assignment is evident from figure **S11** where differential electron density (DED) map is superimposed to the proposed model and plotted in points within values of -0.6 and 0.55 eÅ$^{-3}$ with a level of 0.2 eÅ$^{-3}$, colored in red for negative and green for positive values respectively. Negative electron density is located on the oxygen at the C8 position while positive electron density is located on the nitrogen at the C7 position. In addition, the first Q-peak (*i.e.* the highest not modelled peak of electron density) reported as a transparent orange sphere is located at approximately 1 Å away from the oxygen atom which is symptomatic of a not assigned hydrogen atom. On the other hand, the hydrogen atom of the amine group not involved in the intermolecular S(7) H-bond ring, over-modelled the electron density map. Additional problems in the electron density map are also observed at the oxygen of the carbonyl moiety due to the unmodelled disorder.

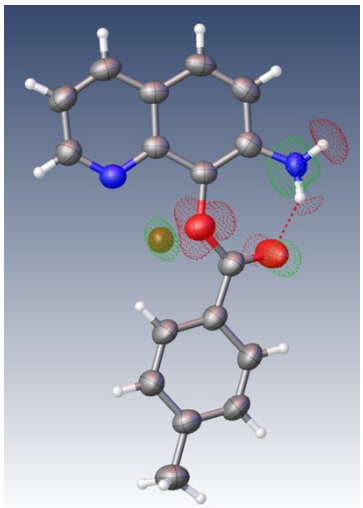

**Figure S11.** Asymmetric unit of the structure solved by Botla et al. and previously reported in the literature with differential electron density (DED) map is superimposed to the proposed model and plotted in points within values of -0.6 eÅ$^{-3}$ and 0.55 eÅ$^{-3}$, colored in red for negative and green for positive values respectively. Superimposed structural models are reported with non-hydrogen atoms in ellipsoids style at 50% level of probability according to the colour code C=grey, N=blue, O=red. Hydrogen atoms are reported in ball-and-stick style for the sake of clarity. The highest unmodelled electron density peak is plotted in transparency.

We further decided to demonstrate that the product previously reported in the literature was consistent with the reaction mechanism here proposed by re-refining the structure against the raw data included in the deposited cif file in the CSD (ref code VIXMAT). In figure **S12** it is reported a comparison of the differential electron density (DED) map between the structured as deposited (left) and the structure as refined according to the C7 oxidation model. After a correct assignment of the atomic positions and the disorder modelling, we obtained a $R_1$=3.96 compared with the $R_1$=6.96 reported in the original structure. In addition, as also described in the main article, the formation of the amide group following the C7 oxidation mechanism is consistent with a further stabilization of the structure due to the formation of an S(7) and an S(5) H-bond rings and, more importantly, we clearly observed a fairly flat DED map (largest difference peak/hole 0.19/-0.12 eÅ$^{-3}$). In Table S5 the crystallographic data of the structures are summarized as deposited and as re-refined by us against the original raw data.

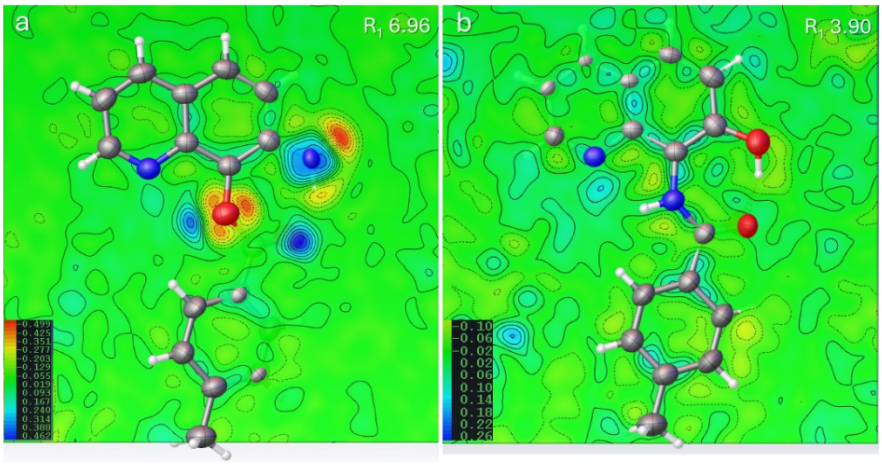


**Figure S12. a.** 2D slices of the differential electron density (DED) map (colored contour style) observed for the structural model a. as originally deposited by Botla et al. [Green Chem 2019, 21, 1735] consistent with the C8-to-C7 amino shift and **b.** according to the further refined model consistent with the C7 hydroxylation. Blue and red areas represent under- vs over- estimation of the modelled electron density, respectively. Color scale is automatically adapted according to maximum and minimum values of the map (a. min=-0.499, max=0.462 $e^-/Å^3$; b. min=-0.10, max=0.26 $e^-/Å^3$). Superimposed structural models are reported with non-hydrogen atoms in ellipsoids style at 50% level of probability according to the color code C=grey, N=blue, O=red. Hydrogen atoms are reported in ball-and-stick style for the sake of clarity. All out-of-plane atoms are plotted in transparency.